Particle-in-cell simulations of planar and cylindrical Langmuir probes: Floating potential and ion saturation current

Felipe Iza[a] and Jae Koo Lee[b]
Pohang University of Science and Technology, San-31, Hyoja, Pohang 790-784, South Korea

(Received 4 May 2005; accepted 22 February 2006; published 22 June 2006)

Particle-in-cell and hybrid electron-Boltzmann simulations of planar and cylindrical Langmuir probes are compared with various probe theories. Floating potentials for planar and cylindrical probes are calculated and significant deviations from the typical approximation used for argon discharges of $\sim 5T_e$ are shown. The interpretation of simulated ion saturation currents by the orbital motion limited and the Laframboise theories result in an overestimation of the ion density. On the other hand, the cold-ion theory underestimates the ion density. These deviations are related to the overestimation and underestimation, respectively, of the ion orbital motion around cylindrical probes. The best agreement is obtained when the probe theory suggested by Tichy *et al.* is used. This theory incorporates ion orbital motion as in the Laframboise theory, collisional orbital motion destruction as suggested by Zakrzewski and Kopiczynski, and ion scattering as given by Chou*et al.* © *2006 American Vacuum Society.* [DOI: 10.1116/1.2187991]

I. INTRODUCTION

Langmuir probes[1–3] provide a means for determining the plasma density and the electron energy distribution function with a spatial resolution of a few Debye lengths. Langmuir probe measurements, however, are challenging both from an experimental and a theoretical point of view. Experimentally, one has to deal with the consequences of having a probe in direct contact with the plasma and biased to an available reference electrode. In this work, however, we focus on the theoretical problem, i.e., interpreting the current-voltage characteristic of the probe. The main three collisionless probe theories are the orbital motion limited (OML),[4] the cold-ion theory of Allen-Boyd-Reynolds (ABR),[5–7] and the Bernstein-Rabinowitz-Laframboise (BRL) theory.[8,9] These theories have been expanded to include the effects of ion collisions although up to date there is not one unified theory.[10–16] The problem of interpreting the probe measurement is intimately related to that of the sheath formation which is also rich in complexity as the extensive existing literature suggests.[17–24]

Despite the potential of particle-in-cell (PIC) simulations, limited literature can be found in which this simulation technique had been used to analyze probe theories. Kwok *et al.* have simulated the sheath formation in a drifting plasma[25,26] and Hrach and Vicher in a pulsed plasma.[27] Trunec *et al.* have analyzed the electron and ion collection current by a cylindrical probe separately using a test particle method (tracing particles in a predetermined spatial potential profile).[28,29] Taccogna *et al.* have studied the ion collection current assuming a Maxwellian distribution of electrons and solving Poisson's equation to determine a self-consistent spatial potential profile.[30] Bergmann[31] and Soberon[32] have used a particle-in-cell approach (electrons and ions) to simulate a planar Langmuir probe in a magnetized plasma and a cylindrical probe in an unmagnetized plasma, respectively.

In this work, we compare Langmuir probe simulation results obtained using a PIC Monte Carlo collision (MCC) and hybrid electron Boltzmann-PIC models with the OML (Ref. 4) theory, the cold-ion theory of ABR,[5–7] and the BRL theory.[8,9] Additionally, a comparison is made with the collisional theory proposed by Tichy *et al.*[13] This theory incorporates ion collisions in the BRL theory by taking into account the destruction of ion orbital motion as suggested by Zakrzewski and Kopiczynski[12] and the ion scattering given by Chou *et al.* and Talbot and Chou.[10,11]

PIC simulations do not require a separation between bulk plasma, sheath, presheath, and/or transitions regions. In fact, these terms have been used with different meanings by different authors leading to more than a decade of controversy.[19,20] In this work we shall refer as sheath to the region surrounding the probe where positive space charge exists, i.e., this region includes the Child-Langmuir sheath (also referred in the literature as the ion sheath) where the electron density is negligible, and the transition region where the electron density cannot be neglected but quasineutrality can neither be applied. The sheath defined in this way is delimited by the probe and a fictitious boundary that we shall refer as the sheath edge (this sheath edge corresponds to the "plasma edge" as defined in Ref. 20). Our sheath edge marks the point where quasineutrality breaks, i.e., $(n_i - n_e)/n_i = \varepsilon$ with $0 < \varepsilon \ll 1$. Here n_i and n_e are the ion and electron densities, respectively. The point where quasineutrality breaks, however, is ill defined as the electron density is lower than the ion density everywhere in the plasma. In this paper we have set the sheath edge at the point where $\varepsilon = 0.015$. This value has been selected not in the spirit of making a new sheath boundary definition but rather with the intention of closely determining the point where quasineutrality breaks while overcoming the intrinsic noise in the density profiles obtained in particle simulations. The sheath edge defined in

[a]Electronic mail: fiza@postech.ac.kr
[b]Electronic mail: jkl@postech.ac.kr

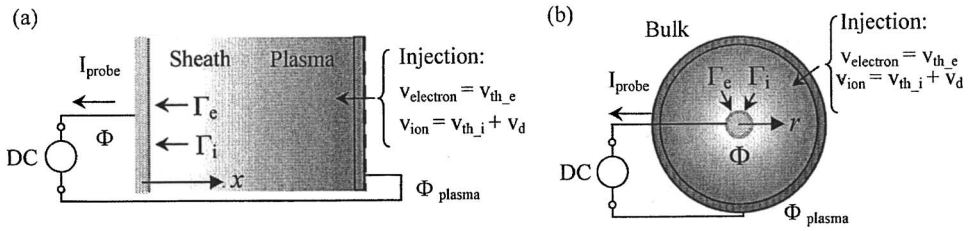

FIG. 1. Schematic of the systems being modeled. (a) Planar geometry: one-dimensional simulation along x direction. (b) Cylindrical geometry: one-dimensional simulation along r direction.

this way is a good indicator of the point where the space charge sheath starts developing. More importantly, it is a definition that is independent of the collisionality of the discharge (sheath and presheath) and therefore it can be equally applied to all the simulated cases. At the sheath edge ions have a significant drift velocity towards the probe (the Bohm velocity if the sheath is collisionless, lower otherwise). This velocity is acquired in a region that we shall refer as presheath. In the presheath ions are accelerated from a zero drift velocity in the bulk plasma to the drift velocity displayed at the sheath edge. We shall refer as floating potential to the sum of the voltage drop across the sheath and that across the presheath when the probe is left unbiased (open circuit). Note that for a planar geometry, the sheath + presheath model as defined here corresponds to the solution of an infinite plasma slab. This problem has been extensively studied in the literature with different levels of abstraction both analytically and numerically. See, for example, Refs. 17, 19, 22–24, 33, and 34 and references within. Our results agree with existing solutions and extend previous results across various collisionality regimes.

II. SIMULATION MODELS

Two simulation models based on the PIC method[35] have been used to simulate planar and cylindrical Langmuir probes. This simulation technique has been successfully used to study discharge physics, showing its strength in nonequilibrium systems such as low-pressure plasmas where distribution functions are not Maxwellian and nonlocal effects play an important role.[36] Nonetheless, provided that the number of particles is sufficiently large, PIC simulation results correspond to the solution of the Boltzmann equation.[37]

Figure 1 shows a schematic of the planar and cylindrical geometries that have been considered in this work. In both cases, a one dimensional in space and three dimensional in velocity (1D3v) analysis has been performed. Therefore, edge effects at the base and the tip of the probe are neglected. The simulation codes developed for this work are based on XPDP1 and XPDC1,[38] one-dimensional electrostatic bounded plasma simulation codes.

The simulation domain is limited by two boundaries. One of the boundaries is assumed to be the probe and it is either externally driven by an ideal voltage source when simulating a biased probe or left in open circuit when simulating a floating probe. The probe is assumed to be located on the left hand side (LHS) and therefore ions have a negative velocity as they approach the probe. On the right hand side (RHS) boundary, an electrodeless boundary that simulates the bulk plasma is implemented. Electrons and ions are injected every time step through the RHS boundary according to the desired input plasma characteristics. The number of particles being injected is such that the density at the RHS boundary is constant and equal to the desired bulk plasma density. The velocity of the injected particles is obtained by inverting the flux of the desired velocity distribution function of electrons and ions in the bulk.[39] In this work only Maxwellian distributions have been considered, but this could be extended to other distribution functions typically encountered in practice.[24,40]

Once particles are injected in the simulation domain, they are moved according to the Newton-Lorentz equation in a self-consistent electric field until they either escape the simulation domain through the bulk plasma boundary (RHS) or are collected by the probe (LHS). A leap-frog scheme is used for integrating the equation of motion.[35] Particle collisions in the simulation domain are modeled using the null-collision model, a computational efficient scheme of implementing MCCs.[41] Elastic, excitation and ionization electron-neutral collisions, and elastic scattering and charge exchange ion-neutral collisions are included in the model. Although the PIC-MCC scheme allows the simulation of inelastic collisions, incorporating ionization in the Langmuir probe simulations is not trivial. While elastic collisions take place in the whole simulation domain and follow the electron density profile, the number of inelastic collisions decays exponentially from the RHS boundary. Hot electrons are injected at the bulk plasma boundary according to a Maxwellian flux. However, once they undergo an inelastic collision, they lose most of their energy and the electron distribution becomes a cut-off Maxwellian (no electron heating is present in the simulation domain). As a result, the ionization profile depends on the position of the RHS and therefore it cannot be assumed to be representative of the plasma that is being simulated. This could be, however, a good model for a hot-filament multidipole plasma.[42] Although ionization in the sheath can be typically neglected (few electrons are present), ionization in the presheath has a very important role in determining the size and the voltage drop across the presheath.

To include ionization in a consistent way, an alternative hybrid Boltzmann-PIC model has also been developed. In this approach, ions are treated as particles by a PIC scheme whereas electrons are assumed to be Maxwellian and to follow the Boltzmann relation. With these assumptions, the electron velocity distribution is known and the electron density profile is readily available from the potential profile. In this model, ionization is included by adding N_{iz} ions per cell

and time step, where N_{iz} is determined from the product of the local electron density and the ionization frequency. Obviously assuming Maxwellian electrons eliminates the electron kinetic information that can be obtained in a pure PIC simulation. Nevertheless we found this approach reasonable for simulating Maxwellian plasmas with probes biased negatively with respect to the plasma potential. Discrepancies between the PIC and hybrid codes, however, are evident when the probe is biased near the plasma potential or in the electron saturation region.

Unless otherwise noted, the figures presented in this work were obtained using the hybrid Boltzmann-PIC code. Pure PIC simulations agree with the results presented when the ionization mean free path is larger than the simulation domain. When this condition is not satisfied, however, the PIC simulations predict larger presheaths and higher floating potentials.

In order to obtain reliable simulation results, PIC simulations need to meet certain constraints in terms of the number of superparticles, time step, and grid size.[36,43,44] The following criteria were followed in this work when setting up the simulations. The simulation domain was divided in grid cells that resolved the Debye length for the plasma conditions being simulated. The time step was then chosen so that the fastest particle in the simulation domain would not cross a grid cell in one time step (Courant condition) and that the probability of a particle undergoing more than one collision per time step was less than 1%. The number of superparticles was adjusted to yield 100–1000 particles per cell. This required simulations with up to a few million particles.

Finally, it is worth mentioning that unlike in experiments where the probe is typically biased with respect to a grounded chamber, in the simulations the probe is biased with respect to the plasma potential (RHS boundary). Therefore, the floating potential as defined in this work should not be confused with a voltmeter reading of a floating probe with respect to ground in a real setting. Furthermore, the simulations take as input the plasma characteristics, i.e., plasma density, pressure, and electron and ion temperatures. These can be chosen arbitrarily regardless of the chamber size that would be required to generate such a plasma in a real system. This differs from an experimental situation where one is typically bounded to a given plasma chamber and changing one plasma parameter (say pressure) results in changes on the others (electron temperature and plasma density).

III. SIMULATION RESULTS

A. Floating probe: Planar geometry

When a probe is left floating in contact with a plasma, the probe is biased negatively with respect to the plasma potential until the fluxes of electrons and ions impinging on the probe are equal, i.e., zero net current flowing through the probe. If ions are assumed to enter the sheath with the Bohm velocity ($u_B=\sqrt{qT_e/m_e}$) and electrons to be Maxwellian, the floating potential is given by[33]

$$\Phi_f = \Phi_{\text{fsheath}} + \Phi_{\text{fpresheath}} = \frac{1}{2}T_e \ln\left(\frac{M_i}{2\pi m_e}\right) + \ln\frac{n_o}{n_s} \approx 4.7T_e + \ln\frac{n_0}{n_s} \quad \text{for argon}, \tag{1}$$

where M_i is the ion mass, m_e the electron mass, T_e the electron temperature in volts, and n_s and n_o the densities at the sheath edge and the bulk plasma, respectively. For planar probes, the minimum voltage drop across the presheath (Φ_{fp}) is $0.7T_e$.[18] This corresponds to the limiting case of a purely ionizing presheath, i.e., a case where ions are collisionless. The same result is obtained from the analysis of a plasma slab, i.e., at low pressure ($\lambda_i \gg L$), the ratio n_s/n_o converges to 0.5.[33]

Modeling ions in the presheath as a fluid, assuming Maxwellian electrons, invoking current continuity and quasineutrality, and solving the ion momentum balance equation, it can be shown that the voltage across the presheath depends on the collisionality of the presheath and that this collisionality can be measured by a parameter $\alpha=u_B/\nu_{iz}\lambda_{ion}$ where ν_{iz} is the ionization frequency, λ_{ion} the ion mean free path assumed to be constant, and u_B the Bohm velocity.

Based on this model, the potential evolution in a planar presheath as a function of the ion velocity for various collisional regimes can be calculated. The results of such calculations are shown in Fig. 2(a). This figure is similar to that presented by Riemann[18] for the limiting cases of pure collisional ($\alpha\to\infty$), and ionizing ($\alpha=0$) presheaths. In obtaining Fig. 2(a) it has been assumed that ions reach the Bohm velocity at the sheath edge, i.e., that the sheath is collisionless, regardless of the collisionality in the presheath. Although this is not always the case, it exemplifies the role of ionization and collisions in the presheath. As suggested in Fig. 2(a), the presheath region of a planar probe must extend up to a region where ionization is significant (or far enough from the probe up to a point where the planar geometry approximation does not longer hold).

Figure 3 shows the floating potential of planar probes immersed in various argon plasmas at different pressures. It can be observed that the floating potential (sheath+presheath as previously defined) is fairly independent of pressure and plasma density but has a marked dependence on electron temperature. The dependence on electron temperature, however, is not linear [Fig. 3(b)]. For argon plasmas with electron temperatures above ~4 eV, the normalized floating potential (Φ_f/T_e) converges to 5.4. For lower electron temperatures, however, this value increases rapidly. This is a result of the increase of the potential drop across the presheath. As the electron temperature decreases for a given pressure, so does the ionization frequency and ion collisions in the presheath become important (the collisionality parameter α increases with decreasing T_e).

The dependence of the floating potential on the electron temperature and the independence over orders of magnitude on pressure may seem striking and counterintuitive. Based on Eq. (1), this behavior requires the ratio n_o/n_s to be independent of pressure and a function of T_e. It is well estab-

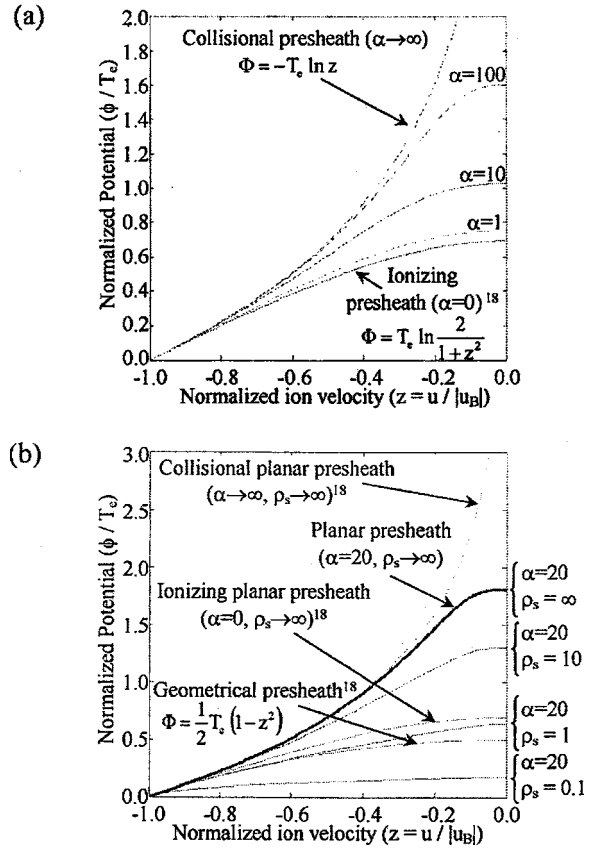

FIG. 2. Potential profile vs ion drift velocity in the presheath region based on a fluid model. (a) Planar geometry and (b) cylindrical geometry. The potential is normalized by the electron temperature and the potential at the sheath edge is taken as a reference. The ion drift velocity is normalized by the Bohm velocity and it is zero at the bulk (right hand side of the figures) and equals the Bohm velocity at the sheath edge (left hand side of the figures).

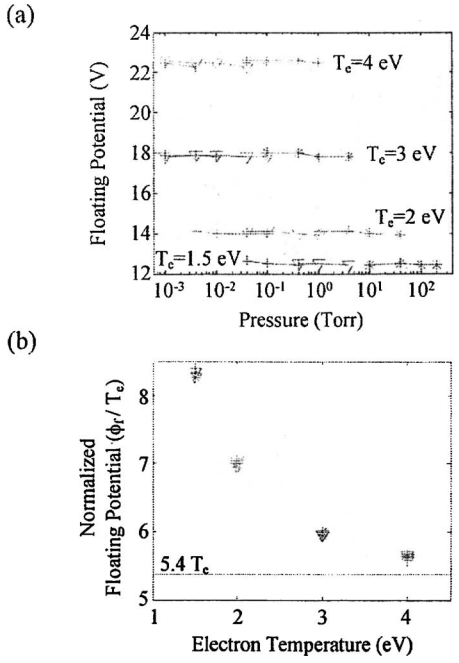

FIG. 3. (a) Floating potential vs pressure for argon plasmas. Symbols represent plasma density: * 10^{14} cm^{-3}, ▽ 10^{11} cm^{-3}, and + 10^{9} cm^{-3}. (b) Same data as in (a) but plotted as normalized floating potential vs electron temperature.

lished that for collisionless sheaths, the ratio n_s/n_o is a function of λ_{ion}/L where λ_{ion} is the ion mean free path and L the plasma size.[33] Although we are used to thinking that this ratio decreases with pressure ($\lambda_{ion} \sim 1/P$), this is only true if L is kept constant. In Fig. 3, however, each trace corresponds to a constant density and a constant electron temperature. Keeping these parameters constant requires changing the size of the discharge (L) with pressure so that ionization and particle losses are balanced.[33] This is hardly achieved experimentally as it would require the change of the plasma reactor as the pressure is increased, but can be easily done numerically to uncouple pressure and electron temperature. This analysis[33] is limited to collisionless sheaths and deviations are expected as pressure increases and both the sheath and the presheath become collisional.

Although the floating potential, i.e., the sum of the voltage drop across the sheath and presheath, is independent of pressure, the contributions of the voltage drops across each region vary with pressure [Fig. 4(d)]. As the sheath becomes collisional, the ion velocity at the sheath edge decreases below the Bohm velocity. As shown in Figs. 4(a)–4(c) the ion velocity at the sheath edge for various plasma conditions can be fitted by

$$u_s = u_B \frac{1}{1 + 5\lambda_{\mathrm{Des}}/\lambda_{\mathrm{ion}}}, \tag{2}$$

where λ_{Des} is the Debye length at the sheath edge. This equation differs from that proposed by Godyak and Sterbeng[23,33] which is also shown for comparison in Fig. 4. The discrepancy is due to a different definition of the sheath edge. In this work, the sheath edge is defined as the point where the electron density is less than 1.5% the ion density, approximately indicating the origin of the space charge sheath. On the other hand, Godyak and Sterbeng define the sheath edge as the point where the electric field reaches a value of $T_e/\lambda_{\mathrm{Des}}$, which is a good indicator of the origin of the ion sheath.[23] In Franklin's nomenclature,[20] we give the ion velocity at the plasma edge while Godyak and Sternberg at the "sheath edge." As one could expect and in agreement with Refs. 20 and 34, we find that such electric field is reached well into the space charge sheath. Using Eq. (2) to determine the ion velocity at the sheath edge and assuming Maxwellian electrons, the voltage across the sheath region for a planar floating probe is given by

$$\Phi_{\mathrm{fs}} = \frac{1}{2} T_e \ln\left(\frac{M}{2\pi m}\right) + \ln\left(1 + 5\frac{\lambda_{\mathrm{Des}}}{\lambda_i}\right). \tag{3}$$

The first term the equation corresponds to the voltage drop assuming that ions enter the sheath with the Bohm velocity while the second term corrects such assumption when the sheath is collisional.

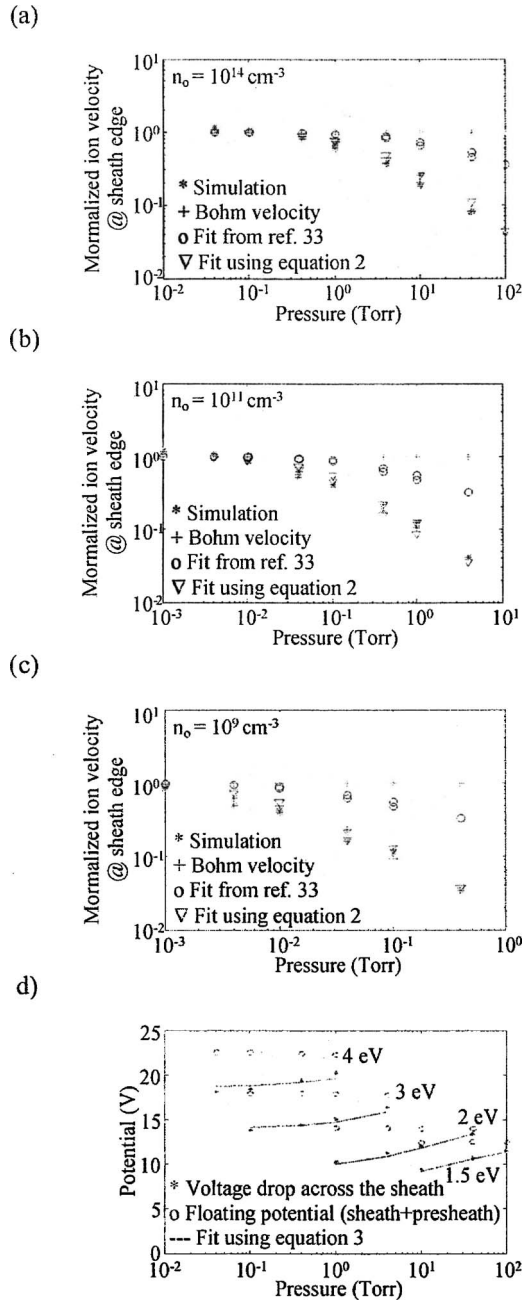

FIG. 4. Ion drift velocity at the sheath edge as a function of pressure for the argon plasmas with plasma densities of (a) 10^{14} cm^{-3}, (b) 10^{11} cm^{-3}, and (c) 10^{9} cm^{-3}. (d) Floating potential (sheath+presheath) and voltage drop across only the sheath for various discharge conditions.

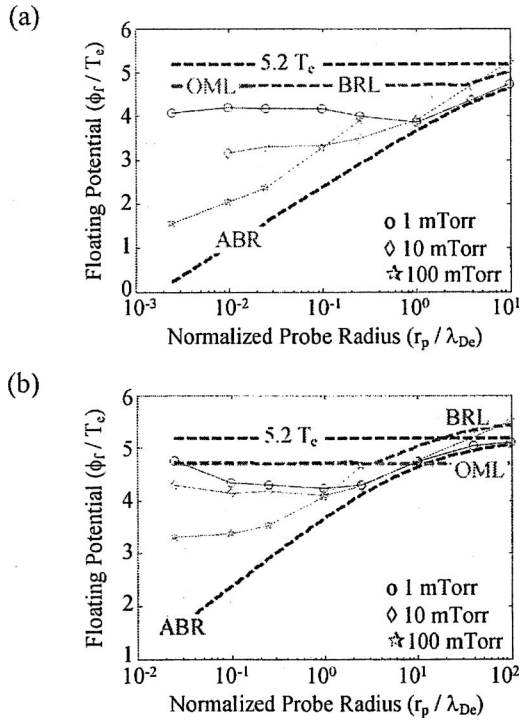

FIG. 5. Normalized floating potential (ϕ_f/T_e) as a function of the normalized probe radius (r_p/λ_{De}) for an argon discharge with (a) $T_e=3$ eV and $n_o=10^9$ cm^{-3} and (b) $T_e=3$ eV and $n_o=10^{11}$ cm^{-3}. The floating potential predicted by the OML, ABR, and BRL theories has been added for comparison. Neither the theories nor the simulations incorporate the role of ionization.

B. Floating probe: Cylindrical geometry

The floating potential of a cylindrical probe immersed in an argon plasma is typically taken as being $5.2T_e$. These results are obtained by assuming a potential drop across the sheath of $4.7T_e$ as given by Eq. (1) (thin sheaths are required to use this result derived for planar probes) and a potential drop across the presheath of $0.5T_e$ (geometrical presheath[18]). As for the planar probe, current continuity and ion momentum balance equations can be solved imposing quasineutrality to get an insight on the potential profile across the presheath in a cylindrical geometry. In this case the potential profile versus ion velocity depends not only on the collisionality parameter α, but also on the curvature of the system ($\rho_s = r_{\text{probe}} + s/\lambda_{\text{ion}}$ where r_{probe} is the probe radius, s the sheath width, and λ_{ion} the ion mean free path).

Due to the geometrical increase of current as ions move towards a cylindrical probe, the voltage drop across the presheath decreases with respect to the planar case. As shown in Fig. 2(b), depending on the system curvature (ρ_s) the voltage across the presheath can be larger than $0.5T_e$ if ρ_s is large and collisions are relevant, or on the contrary almost negligible when ρ_s is small.

Therefore, although the approximation of the floating potential being $5.2T_e$ for argon is convenient and often times valid for rough estimations, the floating potential may significantly deviate from this value.

Alternative to this extrapolation of the result of a planar probe to a cylindrical geometry, Chen and Arnush have derived a parametric equation for the floating potential of cylindrical probe based on the ABR theory.[45] In Fig. 5 a comparison between the planar approximation, the ABR theory, and our simulation results for various probe radius and plasma conditions is presented. Additionally the floating potential predicted by the OML theory and the BRL theory has also been included. As expected, the ABR and BRL theories overlap for a small probe radius ($r_p < 3\lambda_{De}$) and the ABR theory converges to the planar theory ($5.2T_e$) for a large probe radius ($r_p \to \infty$).

For thin probes ($r_p \ll \lambda_{De}$), the floating potential decreases with increasing pressure. At low pressure (1 mTorr) simulation results are closest to the OML and the BRL theories ($\sim 4.7T_e$). As pressure increases, however, the floating potential decreases towards the ABR prediction. This tendency indicates that for thin probes ion collisions favor the ion collection to the probe due to the destruction of orbital motion.

For large probes ($r_p \gg \lambda_{De}$), however, the tendency is the opposite, i.e., the floating potential increases as pressure is increased. As the probe radius increases, the curvature of the system (ρ_s) decreases, orbital motion becomes negligible, and the presheath around the probe widens. As a result, the collisionality of the presheath becomes more important and the collisional drag limits the ion collection. Therefore the effect of ion collisions (pressure) strongly depends on the geometry of the probe (r_p) as well as the plasma density and temperature (λ_{De}).

C. Ion saturation current: Cylindrical probe

By sweeping the probe voltage in the simulations one can obtain *I-V* curves as it is done in experiments. In this case, however, the plasma conditions are known and therefore different theories can be applied to the resulting *I-V* curve to compare their interpretation of the probe trace with the real plasma conditions.

Figure 6(a) shows the ion current obtained from the simulation of a 200 μm radius probe immersed in argon plasma with an electron temperature of 3 eV and a bulk density of 10^9 cm^{-3} at 1, 10, and 100 mTorr. The probe voltage is swept from −50 to 0 V in 100 μs. This time is sufficiently large to allow ions to respond to the applied voltage. Simulation results with a 1 ms sweep time are identical to the ones presented here whereas a reduction of the sweep time to 10 μs results in noticeable differences. It should be remembered that the probe voltage reported is referred to the plasma potential and not to a ground chamber. Therefore the ion current is expected to be close to zero when the applied voltage is zero.

The current traces in Fig. 6(a) present noise due to the limited number of ions that can be simulated. This noise is intrinsic to any PIC simulation and can be reduced by either increasing the number of superparticles or by filtering techniques.[35] As pressure is increased the ion saturation current first increases (see traces for 1 and 10 mTorr) and then decreases (see traces 10 and 100 mTorr). This is in agreement with previous studies that show that initially ion-neutral collisions enhance the ion collection due to the destruction of orbital motion but later reduce it due to the addition drag exerted on the ions.[30,32]

The fits to the ion currents using the parameterization of the OML, the ABR, and the BRL theories given by Chen[46] are also shown in Fig. 6(a). The fits of the OML and the BRL theories are almost indistinguishable as one would expect for a thin probe in a weak plasma. The fit based on the ABR theory is slightly different from the other ones but in any case the three theories fit the data reasonably well. As shown

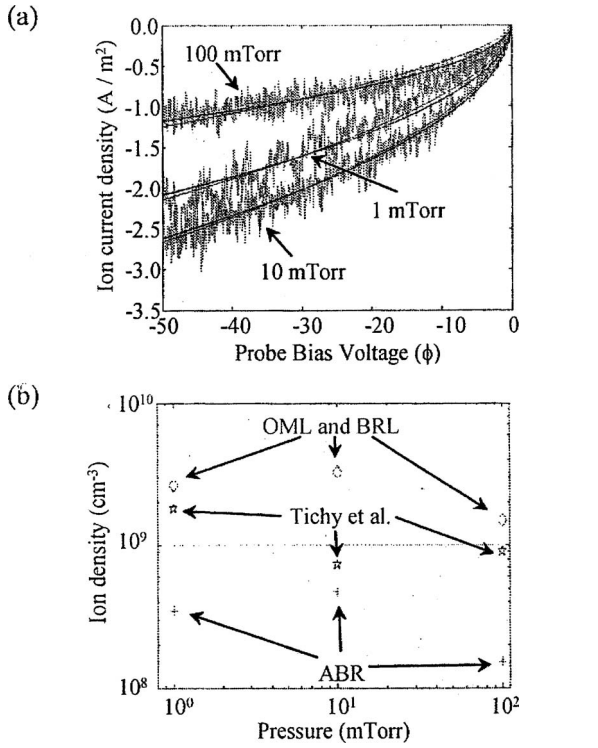

FIG. 6. (a) Ion current density collected by a 200 μm radius probe immersed in an argon plasma ($n=10^9$ cm^{-3} and $T_e=3$ eV) at 1, 10, and 100 mTorr. Fits based on the OML, ABR, and BRL theories are superimposed to each simulation trace. (b) Ion density calculated using the OML, ABR, and BRL theories on the ion current traces shown in (a) and a modified BRL theory as suggested by Tichy *et al.*

in Fig. 6(b), however, the ion density predicted by the three theories is quite different. The OML and the BRL theories overestimate the plasma density whereas the ABR theory underestimates it. Similar trend was obtained by Chen when the interpretation of experimental probe measurements was compared with the average plasma density measured by microwave interferometry.[47] The overestimation of the ion density by the OML and BRL theories is caused by an overestimation on the number of ions that orbit the probe. In a real discharge, ions undergo collisions which reduce the ion angular momentum and thereby increase the ion collection. On the other hand, the ABR theory completely neglects orbital motion and assumes that every ion is collected by the probe. The best agreement is obtained with the collisional theory suggested by Tichy *et al.* that incorporates the ion orbital motion destruction as well as the collisional ion drag due to ion-neutral collisions.[13]

Taking into account the large discrepancy between the different probe theories, the effect of ionization for the cases presented in this work is negligible ($<15\%$). However, it should be mentioned that it is not possible to simulate a collisional plasma without considering ionization unless the presheath region is truncated. If ions are collisional, the presheath of both planar and cylindrical probes extends until a region where ionization is important and therefore the voltage drop across the presheath depends on the heating characteristics of the discharge.

IV. CONCLUSIONS

Particle-in-cell (PIC) Monte Carlo collision and hybrid Boltzmann-PIC codes have been developed to simulate Langmuir probes. Simulation results of planar and cylindrical probes have been presented and compared with various theories. Additionally the kinetic information of ions entering the sheath has also been presented.

Interpretation of simulated cylindrical probe *I-V* curves by the BRL and OML theories results in an overestimation of the plasma ion density whereas the ABR theory underestimates the plasma density. This is a consequence of the overestimation and underestimation, respectively, of the ion orbital motion. As pressure increases, ion collisions initially enhance the ion collection by the probe due to the destruction of orbital motion in the sheath. As pressure continues to increase, however, the destruction of orbital motion is overshadowed by the ion scattering (drag) and the ion collection decreases. A reasonable agreement is found between simulations and the collisional theory suggested by Tichy *et al.* that incorporates the destruction of orbital motion suggested by Zakrzewski and Kopiczynski and the ion scattering given by Chou *et al.*

Although ionization can be neglected in the sheath region where the electron density is small, it must be considered when modeling the presheath if one wants to obtain a self-consistent solution. Ionization across the presheath determines the voltage drop across this region. Although this voltage can be neglected when the probe is strongly biased, it can be significant when the probe is floating or driven near the plasma potential.

Simulation results show that the normalized floating potential (Φ_f/T_e) of planar and cylindrical probes in argon plasmas can significantly deviate from the typically assumed values of 5.4 and 5.2, respectively. For planar probes, the normalized floating potential significantly increases when the electron temperature is lower than $\sim$4 eV. For cylindrical probes, the geometrical current increase as ions approach the probe results in a reduction of the floating potential. For very thin probes, however, the increase in orbital motion limits the ion collection by the probe and eventually sets the floating potential.

ACKNOWLEDGMENT

This work was supported by the Korean Ministry of Science and Technology under the Tera-level Nano Devices Project—21C Frontier R&D Program.

[1]F. F. Chen, *Plasma Diagnostic Techniques* (Academic, New York, 1965), Chap. 4.
[2]N. Hershkowitz, *Plasma Diagnostics* (Academic, Boston, 1989), Chap. 3, Vol. 6.
[3]I. M. Hutchinson, *Principles of Plasma Diagnostics* (Cambridge University Press, Cambridge, 1987), Chap. 3.
[4]H. Mott-Smith and I. Langmuir, Phys. Rev. **28**, 727 (1926).
[5]J. E. Allen, R. L. F. Boyd, and P. Reynolds, Proc. Phys. Soc. London, Sect. B **70**, 297 (1957).
[6]F. F. Chen, J. Nucl. Energy, Part C **7**, 47 (1965).
[7]J. I. Fernandez Palop, J. Ballesteros, V. Colomer, and M. A. Hernandez, J. Phys. D **29**, 2832 (1996).
[8]I. B. Bernstein and I. N. Rabinowitz, Phys. Fluids **2**, 112 (1959).
[9]J. G. Laframboise, Univ. Toronto Inst. Aerospace Studies Report No. 100, 1966 (unpublished).
[10]Y. S. Chou, L. Talbot, and D. R. Willis, Phys. Fluids **9**, 2150 (1966).
[11]L. Talbot and Y. S. Chou, *Rarefied Gas Dynamics* Academic, New York (1966), p. 1723.
[12]Z. Zakrzewski and T. Kopiczynski, Plasma Phys. **16**, 1195 (1974).
[13]M. Tichy, M. Sicha, P. David, and T. David, Contrib. Plasma Phys. **34**, 59 (1994).
[14]S. A. Self and C. H. Shih, Phys. Fluids **11**, 1532 (1968).
[15]C. H. Shih and E. Levi, AIAA J. **9**, 1673 .(1971).
[16]Z. Sternovsky, S. Robertson, and M. Lampe, J. Appl. Phys. **94**, 1374 (2003).
[17]S. A. Self and H. N. Ewald, Phys. Fluids **9**, 2486 (1966).
[18]K. U. Riemann, J. Phys. D **24**, 493 (1991).
[19]R. N. Franklin, J. Phys. D **36**, R309 (2003).
[20]R. N. Franklin, J. Phys. D **37**, 1342 (2004).
[21]H. B. Valentini, Plasma Sources Sci. Technol. **9**, 574 (2000).
[22]N. Sternberg and V. Godyak, IEEE Trans. Plasma Sci. **31**, 665 (2003).
[23]N. Sternberg and V. Godyak, IEEE Trans. Plasma Sci. **31**, 1395 (2003).
[24]V. A. Godyak, V. P. Meytlis, and H. R. Strauss, IEEE Trans. Plasma Sci. **23**, 728 (1995).
[25]D. T.-K. Kwok, T. W. H. Oates, D. R. McKenzie, and M. M. M. Bilek, IEEE Trans. Plasma Sci. **31**, 1044 (2003).
[26]D. T. K. Kwok, M. M. M. Bilek, D. R. McKenzie, T. W. H. Oates, and P. K. Chu, IEEE Trans. Plasma Sci. **32**, 422 (2004).
[27]R. Hrach and M. Vicher, Czech. J. Phys. **51**, 557 (2001).
[28]D. Trunec, M. Holik, P. Kudrna, O. Bilyk, A. Marek, R. Hippler, and M. Tichy, Contrib. Plasma Phys. **44**, 577 (2004).
[29]D. Trunec, P. Spanel, and D. Smith, Contrib. Plasma Phys. **42**, 91 (2002).
[30]F. Taccogna, S. Longo, and M. Capitelli, Contrib. Plasma Phys. **44**, 594 (2004).
[31]A. Bergmann, Phys. Plasmas **1**, 3598 (1994).
[32]L. Oksuz, F. Soberon, and A. R. Ellingboe, J. Appl. Phys. **99**, 013304 (2006).
[33]M. A. Lieberman and A. J. Lichtenberg, *Principles of Plasma Discharges and Materials Processing*, 2nd edition (Wiley, New York, 2005).
[34]I. D. Kaganovich, Phys. Plasmas **9**, 4788 (2002).
[35]C. K. Birdsall and A. B. Langdon, *Plasma Physics via Computer Simulation* (McGraw-Hill, New York, 1985).
[36]H. C. Kim, F. Iza, S. S. Yang, M. Radmilovic-Radjenovic, and J. K. Lee, J. Phys. D **38**, R283 (2005).
[37]S. Longo, Plasma Sources Sci. Technol. **9**, 468 (2000).
[38]J. P. Verboncoeur, M. V. Alves, V. Vahedi, and C. K. Birdsall, J. Comput. Phys. **104**, 321 (1993).
[39]K. L. Cartwright, J. P. Verboncoeur, and C. K. Birdsall, J. Comput. Phys. **162**, 483 (2000).
[40]V. A. Godyak, R. B. Piejak, and B. M. Alexandrovich, J. Appl. Phys. **73**, 3657 (1993).
[41]V. Vahedi and M. Surendra, Comput. Phys. Commun. **87**, 179 (1995).
[42]L. Oksuz and N. Hershkowitz, Plasma Sources Sci. Technol. **14**, 201 (2005).
[43]C. K. Birdsall, IEEE Trans. Plasma Sci. **19**, 65 (1991).
[44]E. Kawamura, C. K. Birdsall, and V. Vahedi, Plasma Sources Sci. Technol. **9**, 413 (2000).
[45]F. F. Chen and D. Arnush, Phys. Plasmas **8**, 5051 (2001).
[46]F. F. Chen, Phys. Plasmas **8**, 3029 (2001).
[47]F. F. Chen and J. P. Chang, *Lecture Notes on Principles of Plasma Processing* (Kluwer/Plenum, New York, 2003).